Applied Materials Today 47 (2025) 102929

Contents lists available at ScienceDirect

Applied Materials Today

journal homepage: www.elsevier.com/locate/apmt

Tuning silica acidity with ammonium fluoride: Boosting iridium catalyst performance in furfural hydrogenation

Robert Wojcieszak [a], Monika Kot [b], Arthur Reymond [a], Camila Palombo Ferraz [c], Nikolaos Dimitratos [d], Alberto Villa [e], Ilaria Barlocco [e], Silvio Bellomi [e], Mariusz Pietrowski [b], Ewa Janiszewska [b], Michał Zieliński [b,*], Almudena Marti [a,*]

[a] Université de Lorraine, CNRS, L2CM UMR 7053, F-54000 Nancy, France
[b] Faculty of Chemistry, Adam Mickiewicz University, Uniwersytetu Poznańskiego 8, 61-614 Poznań, Poland
[c] Instituto de Química, Universidade Federal do Rio de Janeiro, Av. Athos da Silveira Ramos, 149, Rio de Janeiro, Brazil
[d] Dipartimento di Chimica Industriale "Toso Montanari", Alma Mater Studiorum Università di Bologna, Viale Risorgimento 4, 40136 Bologna, Italy
[e] Dipartimento di Chimica, Università degli Studi di Milano, via Golgi 19, I-20133, Milano, Italy

ARTICLE INFO

Keywords:
Furfural hydrogenation
Iridium catalysts
Surface Acidity
Amorphous silica
Catalyst characterization

ABSTRACT

This work reports a strategy to enhance iridium-catalyzed furfural hydrogenation by tuning the acidity of amorphous silica supports via ammonium fluoride treatment. The NH_4F treatment induced controlled silicon leaching, which increased the pore volume and generated additional Lewis acid sites, thereby promoting superior metal dispersion. Among the catalysts, Ir-SiO-1.0F achieved nearly complete furfural conversion (>95%) with ~100% selectivity toward furfuryl alcohol, clearly outperforming both unmodified and over-fluorinated systems. Structure–activity correlations revealed that the optimal Ir dispersion (~40%, particle size ~3 nm) and a balanced Ir^0/Ir^{4+} ratio are decisive for high selectivity. XPS and NH_3-TPD measurements demonstrated that acidity and Ir oxidation states act synergistically to favor carbonyl hydrogenation while suppressing ring saturation. Density functional theory (DFT) calculations confirmed the preferential adsorption of furfural on IrO_2. Dual-site top (perpendicular) adsorption of furfural on the IrO_2 surface enables its selective hydrogenation to furfuryl alcohol, with hydrogen dissociating on metallic iridium. These findings establish NH_4F-treated silica as a versatile support design and provide a clear framework for tailoring catalysts for the selective upgrading of biomass.

1. Introduction

Hydrogenation has played a foundational role in industrial catalysis since the late 19th century, when Sabatier's pioneering work demonstrated the utility of nickel as an effective catalyst for the addition of hydrogen to unsaturated hydrocarbons [1–2]. One of its significant modern applications, the hydrogenation of benzene to cyclohexane, is crucial for synthesising nylon intermediates. This underscores the continuing importance of this reaction pathway in today's chemical manufacturing industry. The efficacy of hydrogenation catalysts is governed not only by the nature of the active metal phase but also by the physicochemical properties of the support [3]. Parameters such as surface acidity, crystallinity, and porosity can significantly influence the metal dispersion, reducibility, and overall availability of active sites. Acidic supports, in particular, have been reported to enhance the hydrogenation of aromatic compounds when compared to neutral materials like silica [4–5]. However, supports with strong acid sites, such as zeolites, may also promote competitive side reactions, which can accelerate catalyst deactivation through mechanisms such as coking or structural degradation [6]. Therefore, rational selection and engineering of catalyst supports are essential for achieving a balance between catalytic activity and long-term stability in hydrogenation processes.

The catalytic upgrading of biomass-derived molecules has garnered increasing attention as a sustainable and environmentally responsible alternative to fossil-based chemical production. Among these key platform molecules, furfural, obtained via hemicellulose hydrolysis, represents a versatile intermediate for producing a range of fuels and fine chemicals (Scheme 1). Selective hydrogenation of furfural into value-added compounds such as furfuryl alcohol and tetrahydrofurfuryl alcohol is of particular industrial relevance [7–9]. Nonetheless,

* Corresponding authors.
E-mail addresses: michal.zielinski@amu.edu.pl (M. Zieliński), almudena.marti-morant@univ-lorraine.fr (A. Marti).

https://doi.org/10.1016/j.apmt.2025.102929
Received 13 May 2025; Received in revised form 8 September 2025; Accepted 14 September 2025
Available online 19 September 2025

achieving high catalytic activity and selectivity under mild conditions remains a significant challenge. This difficulty arises from furfural's multifunctional nature, which includes both an aldehyde and a furan ring, making it prone to various side reactions such as ring hydrogenation, polymerisation, or decarbonylation. These competing pathways can compromise both yield and catalyst longevity, thereby necessitating the development of advanced catalytic systems capable of fine-tuned selectivity and enhanced stability.

Heterogeneous catalysts comprising noble metals supported on high-surface-area oxides are widely employed for such transformations. Iridium (Ir) based catalysts, in particular, have demonstrated promising hydrogenation activity due to their high hydrogen dissociation efficiency and tolerance toward polar functional groups (**Table S1**). Nevertheless, catalytic performance is significantly influenced by the physicochemical properties of the support. Attributes such as surface area, acidity, and metal-support interactions play crucial roles in modulating the activity, selectivity, and stability of the active phase [10–12]. Silica is a common catalyst support due to its thermal stability and high surface area, but its lack of acidity can limit catalytic efficiency. Recent studies have shown that modifying the acid-base properties of silica can enhance metal dispersion and improve interactions with polar substrates such as furfural [8,10]. Iridium nanoparticles supported on silica are increasingly utilized as catalysts for various hydrogenation reactions, including the hydrogenation of furfural to furfuryl alcohol. While these catalysts exhibit notable catalytic activity, several limitations affect their overall efficiency and applicability. One significant limitation of Ir/SiO_2 catalysts is the tendency for Ir nanoparticles to agglomerate during catalytic reactions. This phenomenon leads to a loss of active surface area, diminishing catalytic performance over time. Moreover, the low thermal stability of Ir on silica supports makes them susceptible to high-temperature sintering, further impeding performance efficiency. Although much attention has been paid to the catalyst systems, deactivation of the catalysts becomes the biggest hindrance for the development of the catalysts. All the catalysts reported in the literature suffered severe deactivation during the reaction process. The deactivation is mainly due to the high surface activity of the catalyst, which would cause a rapid coke formation and consequently block the active sites [13]. Some authors attributed the deactivation of Ir/TiO_2 catalyst to the formation of strongly chemisorbed asymmetric carboxylates and the formation of heavy products, with conjugated C=O and C=C bonds. Also, decarbonylation of aldehyde moiety and consequently the irreversible adsorption of CO on the metal surface is the reason for the loss of activity due to a poisoning effect [14,15]. In addition, Ir/SiO_2 catalysts often exhibit challenges related to product selectivity. The catalytic activity of Ir can lead to competitive reactions that favour the formation of various hydrogenated products rather than the desired furfuryl alcohol. This selectivity issue can result from the electronic and geometric configurations of the catalytic sites, which may not favour the specific hydrogenation pathway required for efficient furfuryl alcohol production. The interaction between Ir nanoparticles and the SiO_2 support also presents challenges. The weak metal-support interaction can lead to significant leaching of Ir from the support during catalytic cycling. This leaching not only reduces the active catalyst amount but can also result in unforgiving reaction environments leading to transient deactivation. Furthermore, the low adsorption energy of intermediates on SiO_2-supported Ir can hinder effective chemisorption of reactants, thus affecting overall catalytic activity.

Thus, the main objective of this work is to modify the SiO_2 in order to improve the interaction between Ir nanoparticles and the support and increase the stability of the Ir active phase. This paper aims to conduct detailed research to investigate the effects of ammonium fluoride modification on the physicochemical and catalytic properties of amorphous silica. The study explores the influence of the concentration of ammonium fluoride on the support texture and the nature of active sites. The modified silica materials were used as supports for iridium catalysts, and the effect of their acidity on the activity of iridium catalysts for selective furfural hydrogenation was studied.

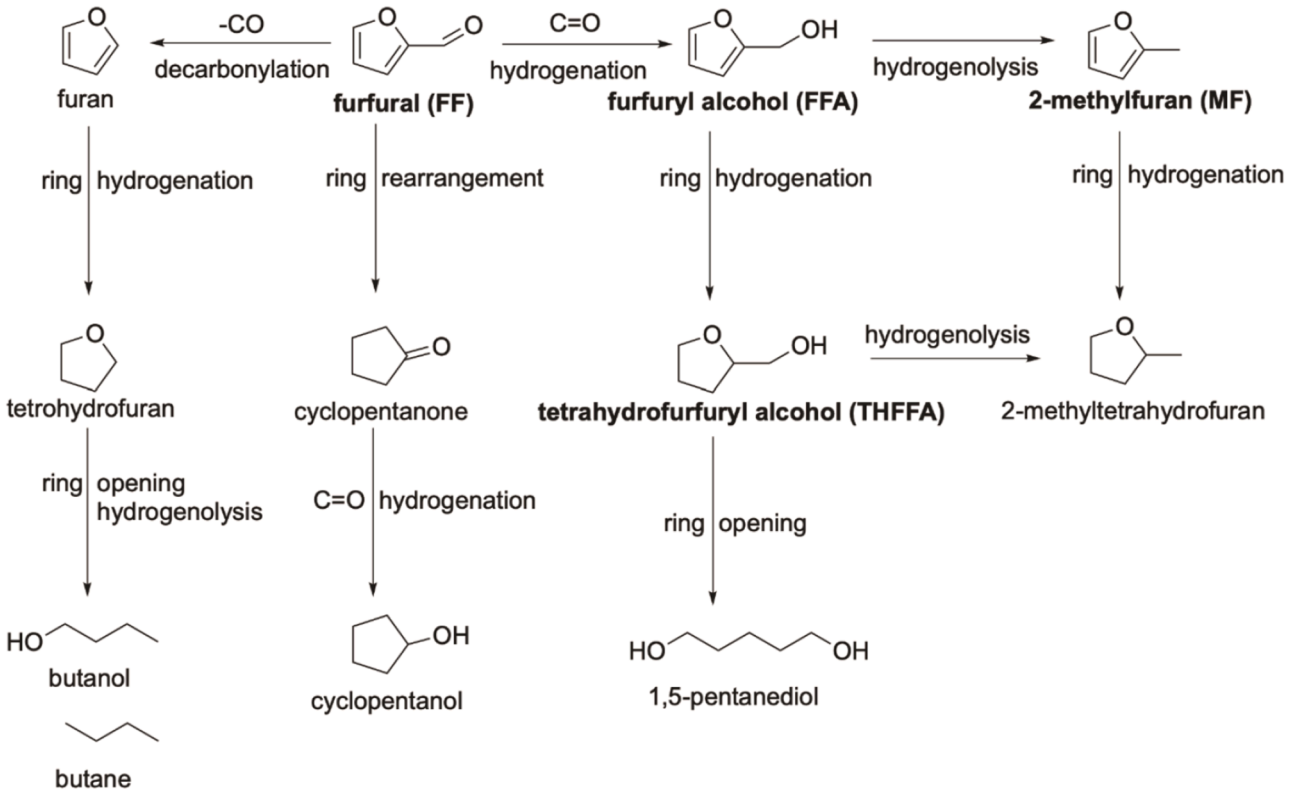

Scheme 1. Reductive conversion of furfural to chemicals and fuels.

2. Experimental section

2.1. Supports and catalysts preparation and activation

Amorphous silica (Polish Chemicals Reagents) was modified with solutions of ammonium fluoride with different concentrations (0.5, 1.0, and 2.0 M). Before modification, the silica was calcined for 3 hours at 550°C. A portion of 1 g of silica was mixed with 100 cm^3 of ammonium fluoride solution of a specific concentration. The obtained mixture was stirred under reflux at 60°C for 1 h. After the treatment, the samples were filtered, washed with hot deionized water, dried at room temperature (RT), and then calcined in the air at 550°C for 3 h. Washing with hot water removes residual ammonium fluoride as well as soluble silicon fluoride species formed during the NH_4F treatment. The resulting samples were labelled as SiO-xF, where x means the concentration of the ammonium fluoride solution used. For comparison, the unmodified silica (labelled as SiO-0F) was also used as a support.

Iridium was deposited on activated (3 h, 550°C) silica supports by the conventional impregnation method using iridium acetylacetonate (Sigma-Aldrich) as a metal precursor. The required quantity of $Ir(acac)_3$ was dissolved in methanol, and the solution was added to the calcined support (the amount of precursor was calculated to achieve an iridium loading of 1 wt.%). After stirring for 30 min, the solvent was removed using a rotary evaporator, and the catalysts were dried at 60 °C for 24 h. The obtained materials were labelled as Ir/SiO-xF-D.

Prior to the measurements of hydrogen chemisorption, as well as before the measurements by low-temperature nitrogen adsorption/desorption (BET), X-ray powder diffraction (XRD), and X-ray photoelectron spectroscopy (XPS) measurements, each precursor-impregnated support was placed in a fixed-bed flow reactor and reduced in hydrogen flow (Linde, 50 cm^3/min). All catalysts were reduced with H_2 at 400 °C for 2 h. The reduced catalysts were labelled as Ir/SiO-xF.

2.2. Supports and catalysts characterization

2.2.1. X-ray diffraction analysis (XRD)

The X-ray powder diffraction analysis was performed on a Bruker AXS D8 Advance diffractometer with Ni-filtered CuKα radiation (λ=1.54056 Å) in the 2Θ range of 10–60°.

2.2.2. Determination of surface area and porosity

The Brunauer-Emmett-Teller (BET) specific surface areas (SSA) were determined by N_2 adsorption at -196 °C using a Micromeritics ASAP 2010 sorptometer. Total pore volume and average pore radius were determined by the Barrett-Joyner-Halenda (BJH) method based on the desorption branch of the isotherm. Prior to the measurements of adsorption-desorption isotherms, the samples were outgassed at 275°C for 4 h.

2.2.3. Temperature-programmed desorption of ammonia (TPD-NH_3)

The temperature-programmed desorption of ammonia measurements (TPD-NH_3) were carried out in order to determine the acidity of the silica supports. The measurements were performed using a Pulse ChemiSorb 2705 apparatus (Micromeritics). In the typical experiment, a sample (~500 mg) was heated in He (99.999%, Linde) at the rate of 10°C/min up to 500°C and then maintained at this temperature for 1 h. Afterwards, it was cooled to 100°C and saturated with ammonia for 30 min. After purging with helium flow at 100°C for 1 h, the TPD-NH_3 analysis was performed in the temperature range of 100–500°C with a heating rate of 10°C/min using a TCD detector. All TPD-NH_3 profiles presented in this work were normalized to equal mass of the sample (1 g).

2.2.4. FTIR analysis

FTIR analysis of pyridine (Sigma-Aldrich) adsorption was performed on self-supported wafers using a FTS 3000 Bio-Rad (Bio-Rad, CA, USA) spectrophotometer connected to a conventional vacuum system. Before FTIR studies, all support samples were activated *in situ* in an FTIR cell at 275°C under vacuum for 90 min. Pyridine adsorption (6.0 mbar) was carried out at 50°C for 10 min, and the spectra were recorded after evacuation at 50, 75, and 100°C for 30 min.

2.2.5. Temperature-programmed reduction with hydrogen (TPR-H_2)

Measurements of temperature-programmed reduction with hydrogen (TPR-H_2) were carried out on a Pulse ChemiSorb 2705 (Micromeritics) instrument. Dried metal precursor-impregnated supports - Ir/SiO-xF-D (~50 mg) were reduced in the flow of 10 vol.%. H_2 – Ar (99.999%, Linde) at the flow rate of 30 cm^3/min. The measurements were conducted in the temperature range from 50 to 700°C at a linear temperature ramp of 10°C/min. The products of the reduction were retained by a cold isopropanol (cold trap at about −70°C). All TPR-H_2 profiles, presented in this work, have been normalized to the same sample weight (100 mg).

2.2.6. Determination of metal dispersion by hydrogen and carbon monoxide chemisorption

The measurements of hydrogen or carbon monoxide chemisorption on supported metal catalysts were conducted by the static method at 35°C (hydrogen) or 100°C (carbon monoxide) on a Micromeritics ASAP2010C sorptometer. Prior to hydrogen/carbon monoxide chemisorption, fresh dried catalysts were reduced with H_2 at 400°C for 2 h and then the catalyst samples were pretreated *in situ* to purify their surfaces from adsorbed gases. The pretreatment consisted of the evacuation at room temperature for 15 minutes and then at 360°C for 60 minutes, followed by reduction in hydrogen flow (40 cm^3/min, 99.999%, Linde) at 360°C for 60 minutes and evacuation at 360°C for 120 minutes. Iridium dispersion was calculated from the irreversibly adsorbed hydrogen or adsorbed CO. From the volume of adsorbed hydrogen/carbon monoxide corresponding to monolayer coverage (v_m), the metallic surface area *(S)*, expressed in m^2/g_{Ir}, was calculated using the following equation [16]:

$$S = \frac{v_m \cdot N_A \cdot n \cdot a_m \cdot 100}{22414 \cdot m \cdot wt} \quad \text{(Eq. 1)}$$

where v_m – volume of adsorbed hydrogen/carbon monoxide (cm^3), N_A is Avogadro's number ($6.022 \cdot 10^{23}$ mol^{-1}), n - chemisorption stoichiometry (n=2 for H_2 or n=1 for CO), a_m – surface area (m^2) occupied by a metal atom, m – the sample mass (g), wt (%) – iridium loading.

The dispersion *(D)* of iridium was calculated from the formula:

$$D = \frac{S \cdot M}{a_m \cdot N_A} \quad \text{(Eq. 2)}$$

where S – the metallic surface area, M – iridium atomic weight, N_A – Avogadro's number and a_m – surface covered by one iridium atom.

The average iridium particle size *(P)*, expressed in nm, was calculated using the following equation:

$$P = \frac{6000}{S \cdot \rho} \quad \text{(Eq. 3)}$$

where S – the metallic surface area, ρ – metal density (g/cm^3).

2.2.7. X-ray photoelectron spectroscopy (XPS)

X-ray Photoelectron Spectroscopy (XPS) analysis of the iridium catalysts was carried out with a Kratos Axis Ultra spectrometer (Kratos Analytical, U.K.). The examined catalysts were irradiated with a monochromatic Al Kα radiation (1486.6 eV). Binding energies were referenced to the C1s peak from the carbon surface deposit at 284.8 eV. The data treatment was performed using CasaXPS Software.

2.2.8. Catalytic test

Furfural hydrogenation was carried out in a Top Industries stainless-steel autoclave reactor at 150°C. In a typical experiment, the reactor was charged with 20 mL of a 0.3 M furfural solution in isopropanol, followed by the addition of the appropriate amount of catalyst to achieve a furfural-to-Ir molar ratio of 500:1. The reactor was sealed and purged three times with H_2 at 10 bar to remove residual air, then pressurized with H_2 to the required pressure (20 bar). Stirring was initiated at 600 rpm, and the reaction start time (t_0) was defined as the point at which the system reached the target temperature (150°C). H_2 pressure was maintained constant throughout the experiment to replenish any gas consumed during the reaction. Unless otherwise stated, reactions were conducted for a total duration of 120 minutes. Reaction products were analyzed using gas chromatography with flame ionization detection (GC-FID) and gas chromatography-mass spectrometry (GC-MS). GC-FID analysis was performed using an Agilent 7890B instrument equipped with a CP-Wax 52 CB column (30 m × 0.25 mm × 0.25 μm). GC-MS analysis was carried out on an Agilent 5977B system, also fitted with a CP-Wax 52 CB column of identical dimensions. The chromatographic program was as follows: the oven was initially held at 37 °C for 4 minutes, ramped at 25 °C/min to 170 °C, then at 50 °C/min to 240 °C, and held at 240 °C for 2 minutes.

The conversion rate (X%) was calculated using the equation:

$$Conversion = \frac{mol_i - mol_f}{mol_i} \cdot 100 \quad \text{(Eq. 4)}$$

where mol_i represents the initial moles of furfural, and mol_f are the moles at the end of the reaction. Selectivity (S%) was determined as follows:

$$Selectivity_a = \frac{mol_a}{\sum mol_n} \cdot 100 \quad \text{(Eq. 5)}$$

where mol_a is the moles of specific product *a* at the end of the reaction, and $\sum mol_n$ is the sum of moles of all the products at the end of the reaction.

2.2.9. Computational methods

Spin-polarized periodic plane-wave DFT calculations were carried out using the Vienna Ab-initio Simulation Package (VASP) [17]. The calculations were performed using projected augmented wave potentials with PBE functionals [18–19], and a cutoff to the kinetic energy for the expansion of the basis set of 400 eV. For the sake of accuracy, non-spherical contributions of the gradient of the density were also included in the PAW spheres [20].

The bulk of Ir and IrO_2 were optimized from reference data using thresholds for electronic energies and ionic forces of 10^{-7} eV and 0.005 eV/Å, respectively. The Brillouin zone was sampled using a 8 × 8 × 8 Γ-centred k-point mesh, obtained *via* the Monkhorst–Pack method, and minimizing any Pulay stress [21]. To study the surface properties and compare the catalytic performance for the furfural adsorption, a $p(3 \times 3)$ Ir (111) and $p(2 \times 4)$ IrO_2 (110) slabs cut from the corresponding optimized bulk system through the Atomic Simulation Environment (ASE) were employed [22], **Fig. S1**. A vacuum of 16 Å along the c-axis was inserted to avoid any interaction between adjacent images. Both the slabs were composed of four atomic layers, with the two uppermost layers left free to relax during the adsorption of furfural, where the convergence criteria were set as 10^{-4} eV and 0.05 eV/Å, and the k-points adapted to the Γ-point. In the adsorption studies, an increased number of initial non-self-consistent steps and linear mixing involving the metal d-orbitals improved the wavefunction convergence, and the Brillouin-zone sampling was eased using the second-order Methfessel–Paxton method with a smearing width of 0.1 eV [23–24]. All the calculations included the long-range dispersion correction approach by Grimme – DFT-D3 methods with Becke-Johnson damping [25–26], an improvement on pure DFT to evaluate molecular interactions [27–28].

The binding energies (ΔE) for each structure (E_S*) were calculated as a difference with the energy of the free trans-furfural (E_{FF}) and surface (E_S), according to the following equation (Eq. (6)):

$$\Delta E = E_{S*} - (E_S + E_{FF}) \quad \text{(Eq.6)}$$

3. Results and discussion

The amorphous silica was treated with ammonium fluoride solutions in order to modify its textural and acidic properties. For this purpose, NH_4F solutions with concentrations of 0.5, 1.0, and 2.0 M were used. An important parameter in the synthesis of new materials is the efficiency of the modification process. The treatment of SiO_2 with fluoride solutions leds to partial leaching of silicon atoms from the silica framework (desilication) and the remaining oxygen atoms interact with hydrogen to form H-bonded silanol defect groups of a different type that serve as acidic centers [29]. This etching process resulted in a measurable mass loss. Specifically, treatment with NH_4F solutions at concentrations 0.5 and 1.0 M caused a mass reduction of approximately 19%, while the use of a 2.0 M solution led to a final mass decrease of around 25%. The XPS analysis demonstrated that all fluoride species were removed during the washing step after modification.

Low-temperature N_2 adsorption-desorption measurements were employed to characterize the textural properties of both unmodified and modified silica samples. The characteristics of the porosity and the specific surface area (SSA) are very important parameters characterizing new supports, influencing the dispersion and particle size of the active phase. Ammonium fluoride treatment of silica resulted in a decrease in SSA, along with an increase in total pore volume (V_t), and average pore size with the increase in modifier concentration - Table 1.

Low-temperature nitrogen adsorption-desorption studies show that the modification caused the generation of additional porosity as the total pore volume increased from 0.69 to 0.95 cm^3/g with an increase in the concentration of the modifier. The initial silica SiO-0F, according to the new IUPAC classification, is characterized by a type IV(a) isotherm with H2(b) hysteresis loop– Fig. 1**a** [30]. The shape of the hysteresis loop (type H2(b)) indicates that the supports have mainly cylindrical pores with a wide neck size distribution, as results from the parallel course of the isotherm adsorption and desorption branches in the range of p/p_0 = 0.6 - 0.8. Such an isotherm is typical for mesoporous materials having a pore system for which network effects are important. Fig. 1**a** displays the adsorption-desorption isotherms of the modified samples. A visible and gradual increase in the adsorbed nitrogen volume at higher values of relative pressure (p/p_0) can be observed with the increase in the concentration of ammonium fluoride solution (from 0.5 to 2.0 M). This phenomenon indicates a gradual increase in the pore diameter with increasing amount of the modifying agent. This can be confirmed by the shift of the maxima on the pore size distribution curves shown in Fig. 1**b**.

Table 1
Physicochemical characterization of the supports.

Support	Mass loss, %	SSA, m^2/g	Total pore volume, cm^3/g	Average pore diameter, nm	TPD-NH_3 $\mu mol_{NH3}/g$	Density of acid sites[a], $\mu mol/m^2$
SiO-0F	-	381	0.69	5.6	9.8	0.03
SiO-0.5F	18.4	355	0.77	7.2	27.2	0.08
SiO-1.0F	19.6	349	0.83	7.5	46.2	0.13
SiO-2.0F	24.8	334	0.95	10.0	46.5	0.14

[a] Concentration of acid centers determined based on TPD-NH_3 measurements.

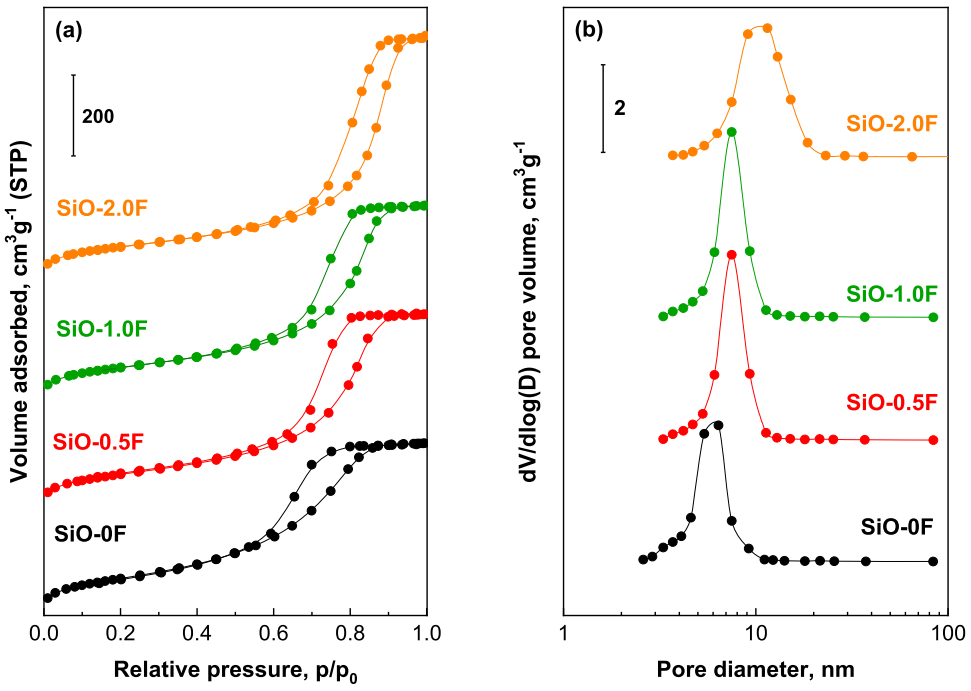

Fig. 1. Low-temperature nitrogen adsorption-desorption isotherms (a) and pore size distributions (b) of silica samples modified with NH_4F solutions.

The non-modified material SiO-0F is characterized by a narrow pore size distribution, mainly in the range of 2-10 nm (with an average pore size of 5.6 nm). An increase in NH_4F concentration results in a reduced contribution of smaller pores and a corresponding increase in the presence of larger pores caused by a partial removal of Si atoms from the silica framework. It is particularly noticeable in the pore size distribution of SiO-2.0F sample characterized with pores in the range of 4-23 nm with a maximum at 10 nm. The modification also results in a decrease in surface area, although this decrease does not exceed 20%, while the average pore diameter nearly doubles - Table 1. The modification of silica with an NH_4F solution initially leads to a 10% decrease in specific surface area (from 381 m^2/g to 355 m^2/g for SiO-0.5F). However, with further increase in the concentration of the modifier used in the modification process, the specific surface area of the obtained materials gradually decreases, reaching a value of 334 m^2/g for SiO-2.0F (Table 1).

To determine acidity, both the starting silica (SiO-0F) and the silica modified with ammonium fluoride solutions were analyzed by temperature-programmed desorption of ammonia (TPD-NH_3) and Fourier-transform infrared spectroscopy (FTIR) with adsorbed pyridine. The results are presented in Fig. 2 (TPD-NH_3 profiles), Fig. 3 (FTIR-Py) and Table 2.

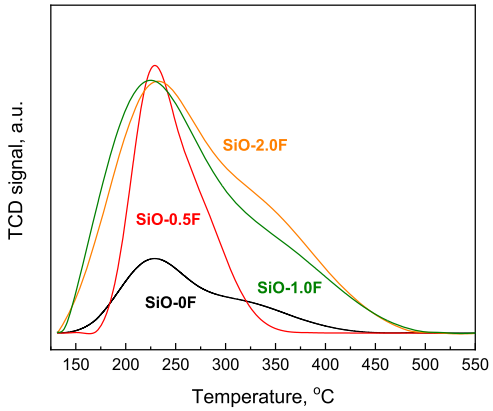

Fig. 2. TPD-NH_3 profiles of the unmodified and modified SiO_2 samples.

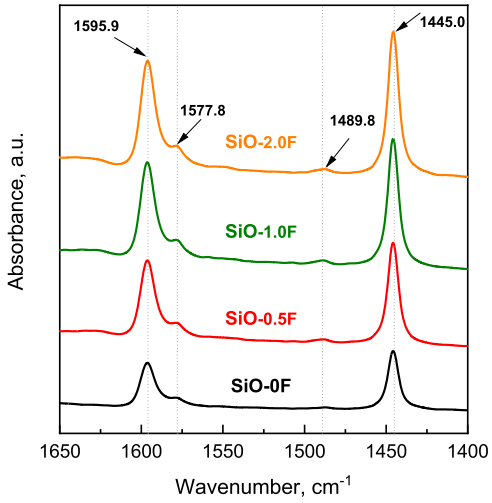

Fig. 3. FTIR spectra of adsorbed pyridine of silica modified with 0.5; 1.0 and 2.0 M NH_4F (evacuation at 50°C).

Based on the TPD-NH_3 profiles, the concentration of surface acid sites was calculated (Table 2), and after deconvolution of the profiles (**Fig. S2**), the concentration of weak and medium acid sites was

Table 2
Acidic properties of amorphous SiO_2 modified with NH_4F solutions of varying concentrations and the initial unmodified silica calcined at 550°C.

Support	Total acidity μmol/g	Content of LT sites, %	Content of HT sites, %
SiO-0F	9.8	42	58
SiO-0.5F	27.2	27	73
SiO-1.0F	46.2	31	69
SiO-2.0F	46.5	43	57

LT- low-temperature sites (below 250°C), HT- high-temperature sites (above 250°C)

evaluated. Modification of the initial support results in the formation of novel hydrogen-bonded silanol groups on its surface that act as acid sites. The number and strength of the generated acid sites depend on the concentration of ammonium fluoride solution used for modification. The starting silica (SiO-0F) exhibits slight acidity (9.8 μmol/g), and modification of its surface with a 0.5 M solution of NH_4F already leads to the generation of additional acidic sites, causing the concentration of acid sites to increase more than twofold. In the case of the sample modified with a 1.0 M solution, a further significant increase in the concentration of acidic sites to 46.2 μmol/g is observed. Further increase in the concentration of the modifying agent does not result in a higher concentration of acidic sites - Table 2.

The shape of the TPD-NH_3 profiles clearly indicates the presence of acid sites of different strengths. According to the traditional classification [31], the deconvoluted peaks (**Fig. S2**) can be classified into two kinds of acid strength corresponding to NH_3 eluted below 250°C (low-temperature acid sites) and above 250°C (high-temperature acid sites). The peaks at higher temperatures (> 250°C) are attributed to the desorption of NH_3 from strong Lewis acid sites, whereas the low temperature peaks are assigned to the desorption of ammonia from weak Lewis acid sites and weakly acidic silanol groups. Based on the deconvolution results, it can be concluded that with an increase in the concentration of the modifying agent, there is an increase in the content of LT acid sites.

The FTIR studies of adsorbed pyridine (Py) allowed to estimate the nature of acid sites in the investigated samples (Fig. 3). The spectra of the starting silica as well as all modified materials show bands characteristic of Py coordinately bounded to Lewis acid sites: ν_{19b} at 1445.0 and ν_{8a} at 1577.8 cm^{-1} [5,32,33]. No bands assigned to Brønsted acid centers was found [34]. The bands at 1445.0 cm^{-1} and 1595.9 cm^{-1} can also originate from pyridine hydrogen-bounded to surface hydroxyl or silanol groups [34,35]. A band at 1577.8 cm^{-1} corresponds to pyridine bounded to weak Lewis acid sites [34,36]. Weak band at 1489.8 cm^{-1}, seen only for the samples after modification, is associated with both Lewis and Brønsted acid sites [36]. Because of the lack of a band at 1532 cm^{-1}, it could be concluded that the band at 1489.8 cm^{-1} originates only from Lewis acid sites. Evacuation at higher temperatures (75 and 100°C) leads to a drastic decrease in the intensity of these bands, indicating weak and medium strength of acidic sites on the surface of the modified samples (**Fig. S3**). This data is in line with TPD-NH_3 results.

It can be observed that the concentration of the ammonium fluoride solution used in the modification process has a significant impact on the intensity of pyridine adsorption bands. A sample modified with a 0.5 M concentration solution is characterized by the presence of pyridine adsorption bands with lower intensity compared to materials modified with solutions of 1.0 or 2.0 M concentration, and the intensity of these bands increases with the concentration of the modifying agent. Changes in the concentration of acidic sites in the modified samples, compared to the concentration of acidic sites in the initial sample, do not correlate with changes in specific surface area (Table 1) as the surface area of the modified samples does not change significantly, while they differ considerably in the concentration of acidic sites, regardless of the method used to estimate them (TPD-NH_3 or FTIR-Py).

The obtained materials were used as supports for iridium catalysts with a surface loading of 1% wt. iridium, introduced using iridium acetylacetonate ($Ir(acac)_3$) as the precursor of the active phase.

Low-temperature nitrogen adsorption-desorption measurements were conducted for catalysts reduced at 400°C for 2 hours. Surface area, average pore diameter, and total pore volume of the investigated catalysts were collected in Table 3. Due to the fact that the nitrogen adsorption/desorption isotherm shapes of the iridium catalysts were very similar to those observed for the supports, it was decided not to show them. Nitrogen adsorption-desorption measurements of the supports showed that the surface area (SSA) of the supports gradually decreases from 381 m^2/g for the unmodified silica (SiO_2) to 334 m^2/g for SiO-2.0F. Similar changes are observed in the case of the surface areas of the iridium catalysts, except that the surface area of the latter is always slightly smaller than the surface area of the corresponding supports. The reduction in the surface area, pore volume, and average pore diameter of the catalysts results from the deposition of the active phase and additional wet and thermal treatments during catalyst preparation.

Table 3
Textural properties of reduced catalysts (H_2, 2 h, 400°C) containing iridium active phase supported on initial silica and silica modified with ammonium fluoride solutions.

Catalyst	Physicochemical characterization of iridium catalysts		
	SSA, m^2/g	Total pore volume, cm^3/g	Average pore diameter, nm
Ir-SiO-0F	367	0.63	5.3
Ir-SiO-0.5F	346	0.75	7.2
Ir-SiO-1.0F	346	0.78	7.4
Ir-SiO-2.0F	329	0.93	9.8

Temperature-programmed reduction (TPR-H_2) was used to determine the temperature required for the reduction of iridium precursor ligands with hydrogen on the catalyst surface. TPR-H_2 studies were conducted on dried samples, and reduction profiles of fresh catalysts dried at 105°C (labelled as Ir-SiO-xF-D) are depicted in Fig. 4.

The TPR-H_2 profiles of iridium precursor ($Ir(acac)_3$) indicate one peak with a maximum at the temperature 277°C with small shoulders at ~300°C (Fig. 4**a**). However, $Ir(acac)_3$ deposited on modified and unmodified silica materials shows hydrogen consumption with two separated maxima at 295°C and 437°C, which indicates two-step decomposition and reduction of the active phase precursor. In the case of supports, reduction peaks were not observed, as the SiO_2, even after modification, is not reducible. According to the authors of [37], thermal decomposition of acetylacetonate ligands in Ir-$acac_x$ species took place at temperatures around 320°C. Based on this information, we can conclude that the maximum reduction at 295°C originates from the decomposition of acac ligands (Fig. 4**b**). The second peak of reduction in the range of 400-450°C, observed in all presented reduction profiles, could be attributed to the reductive decomposition of Ir-$acac_x$ species [37]. In the case of the first reduction peak, besides the maximum at 295°C, a shoulder around ~250°C, attributed to the presence of iridium oxide particles on the catalyst surface, is observed. As reported by the authors [38], this signal can be identified as well-dispersed iridium species. The presence of iridium oxide particles is probably due to the degradation of part of $Ir(acac)_3$ to IrO_2 during drying of the catalysts.

TPR-H_2 studies were conducted to determine the catalysts' reduction temperature. Although complete reduction occurs only at 450°C, the reduction temperature of 400°C used in the study is sufficient for the decomposition and reduction of the precursor to the metallic phase. It should be emphasized that catalyst activation was carried out in pure hydrogen for 2 hours, allowing for the complete transformation of the active phase precursor to metallic iridium. This was confirmed by additional TPR-H_2 measurements of the reduced catalysts, which did not show any reduction peaks, indicating the absence of an unreduced active phase.

An essential factor that governs the catalytic performance of metallic systems is the particle size of the active metal phase. In the present work, this parameter was assessed by means of hydrogen and carbon monoxide chemisorption techniques, which are recognized for their accuracy, particularly when dealing with catalysts containing a low metal loading. The hydrogen chemisorption experiments comprised two types of measurements, enabling the determination of (1) irreversibly adsorbed hydrogen (H_{irr}) and (2) reversibly adsorbed hydrogen (H_{rev}), as reported in Table 4. The former corresponds to hydrogen bound directly to metallic iridium, whereas the latter is attributed to hydrogen species located on the support surface, originating from spillover processes. The total amount of chemisorbed hydrogen (H_t) was calculated as the sum of H_{irr} and H_{rev}. The obtained results demonstrate that H_t considerably

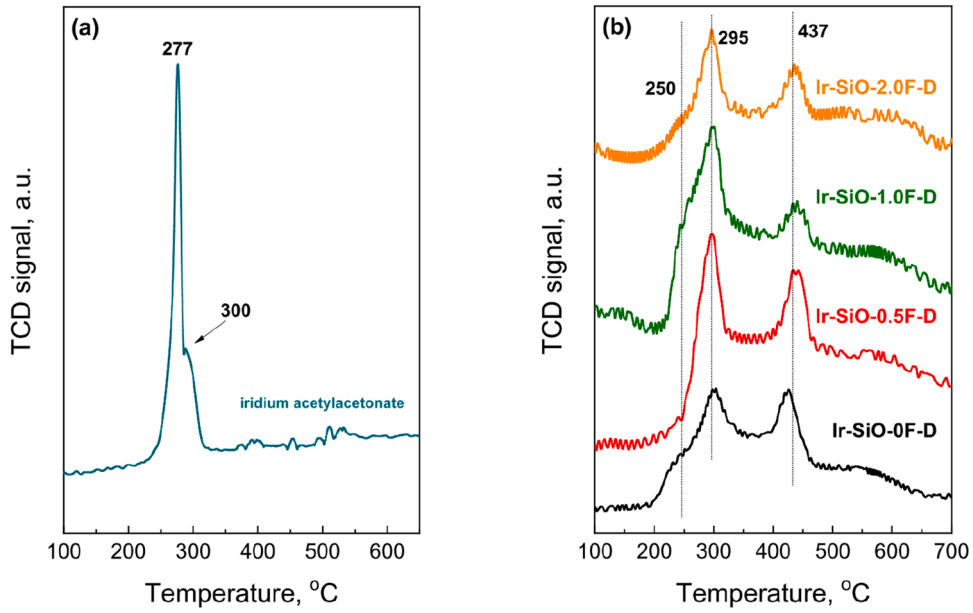

Fig. 4. TPR-H_2 profiles of the iridium precursor Ir(acac)$_3$ (a) and dried iridium catalyst precursors (b). Signal intensity was normalized to 100 mg of catalyst.

Table 4
H_2-chemisorption and CO-chemisorption data of reduced catalysts (H_2, 2 h, 400°C) containing iridium active phase supported on initial silica and silica modified with ammonium fluoride solutions.

Catalyst	H_2-chemisorption data						CO-chemisorption data		
	Volume adsorbed, cm^3/g			Dispersion calculated from H_t, %	Dispersion calculated from H_{irr}, %	Average Ir particle size*, nm	Volume adsorbed, cm^3/g	Dispersion, %	Average Ir particle size **, nm
	H_t	H_{irr}	H_{rev}						
Ir-SiO-0F	0.1705	0.0636	0.1069	29	11	9.3	0.1194	10	10.9
Ir-SiO-0.5F	0.3215	0.1129	0.2086	55	19	5.8	0.2216	19	5.9
Ir-SiO-1.0F	0.5111	0.2279	0.2832	88	39	2.9	0.4397	37	3.0
Ir-SiO-2.0F	0.2652	0.1011	0.1641	45	17	6.5	0.1781	15	7.3

* Mean size of Ir particles (in nm) calculated from the amount of irreversibly chemisorbed hydrogen
** Mean size of iridium particles calculated from the amount of chemisorbed carbon monoxide

exceeds H_{irr}, indicating a major contribution of reversibly chemisorbed hydrogen, most likely associated with the support. In order to validate the dispersion values derived from H_{irr}, complementary chemisorption analyses using carbon monoxide were carried out. In this case, adsorption occurs exclusively on metallic iridium sites. The corresponding values are summarized in Table 4. The dispersion obtained from CO chemisorption showed a close agreement with the estimations based on H_{irr}. Nevertheless, slight discrepancies between the two methods were observed. Such differences can be explained by several factors: (i) CO usually binds more selectively and strongly to particular sites such as edges or steps, while hydrogen tends to adsorb more uniformly, although often with lower affinity and a partially reversible nature; (ii) different adsorption stoichiometries are assumed for both probes - CO is typically considered to adsorb in a 1:1 ratio with surface metal atoms, whereas hydrogen dissociates upon adsorption and may occupy a variable number of sites depending on the surface structure. Furthermore, the stronger interaction of CO with metallic sites often provides a more accurate estimation of dispersion. Consequently, the slightly lower values obtained with CO chemisorption are reasonable and reinforce the reliability of the dispersion derived from hydrogen measurements.

The results of hydrogen and carbon monoxide chemisorption measurements indicate that dispersion of the active phase depends on the textural properties of the support (Table 4). Catalysts supported on modified silica exhibit higher dispersion of iridium particles and smaller iridium particles than the catalyst supported on parent silica. The dispersion of iridium, calculated from irreversibly adsorbed hydrogen or carbon monoxide chemisorption, increases with the concentration of the modifying agent (NH_4F) from ~19% for Ir-SiO-0.5F to ~17% for Ir-SiO-2.0F, reaching the maximum for Ir-SiO-1.0F (40%) – Table 4. The TPD-NH_3 studies conducted on our supports (SiO-1.0F and SiO-2.0F – Table 1) indicated a higher total number of acid centers for SiO-2.0F material. However, the concentration of acid centers expressed per m^2 (Table 1) was comparable for both supports. Fig. 5 shows the correlation of iridium dispersion and the density of acid sites.

Fig. 5 demonstrates that increasing the density of acid sites leads to a decrease in the average Ir particle size, indicating that higher surface acidity enhances the dispersion of the metal phase. This relationship is clearly visible in the Ir-SiO-1.0F sample, which exhibits an acid site density of 0.13 μmol/m^2 and the smallest Ir crystallites (~3 nm, with ~37% dispersion). In contrast, the Ir-SiO-2.0F sample shows a further increase in the total number of acid sites per gram, while its surface density remains essentially unchanged (~0.14 μmol/m^2), comparable to that of Ir-SiO-1.0F. Concurrently, notable changes in the pore structure are observed, particularly a shift toward larger mesopores (~10 nm), as evidenced by nitrogen adsorption isotherms and pore size distributions. This alteration likely facilitates deeper diffusion of Ir precursor species

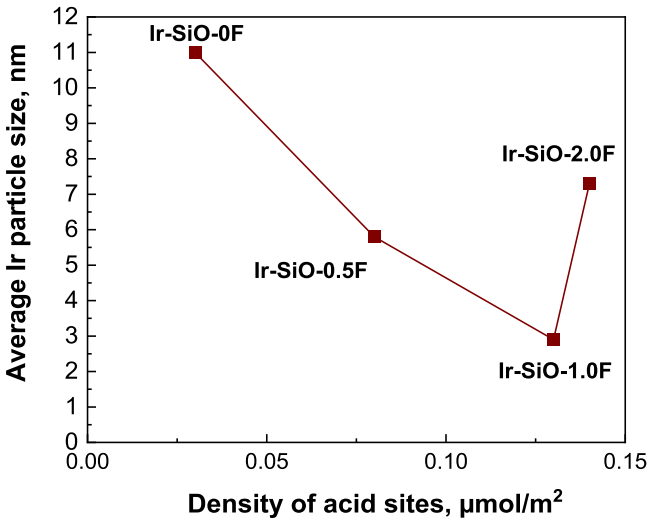

Fig. 5. Correlation of iridium dispersion (average Ir particle size calculated from the amount of chemisorbed carbon monoxide) and the density of acid sites.

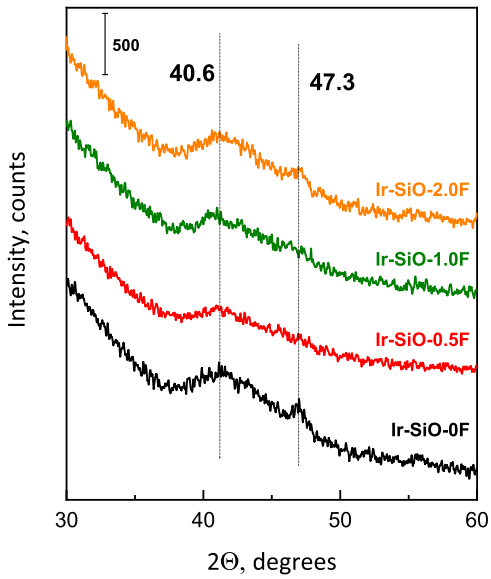

Fig. 6. Wide-angle diffractograms of catalysts containing iridium active phase deposited on modified silicas.

into the support's pores, reducing their interaction with surface anchoring sites and leading to increased particle size and lower dispersion.

The correlation between acid site density and Ir dispersion is supported by both TPD-NH_3 and H_2-chemisorption data, confirming that surface acidity is a critical parameter. Nonetheless, textural characteristics—especially pore size distribution—also exert significant influence. The SiO-2.0F support, with a larger average pore diameter (10.0 nm vs. 7.6 nm for SiO-1.0F), may hinder effective anchoring of Ir precursors during impregnation. These larger pores promote deeper penetration of metal complexes, limiting their interaction with acidic sites and increasing the likelihood of particle agglomeration during drying and reduction. Combined with the absence of further enhancement in acid site density despite the higher NH_4F concentration, these factors likely contribute to the reduced iridium dispersion and the larger crystallite size observed in the Ir-SiO-2.0F sample. Considering both the concentration of acid sites and the textural properties determined by nitrogen adsorption/desorption, it can be concluded that the combination of these properties favours the SiO-1.0F support, for which the smallest iridium crystallite sizes were recorded. Similar observations regarding the beneficial effects of surface acidity as well as porous structure were presented in the literature for modified amorphous silica [32].

The wide-angle XRD measurements were performed to confirm the amorphous character of the silica supports after fluorine modification and to exclude the presence of any crystalline phases other than metallic Ir. The XRD patterns of iridium catalysts (Fig. 6) show only weak reflections at $2\Theta = 40.6^\circ$ (111) and 47.3° (200) corresponding to metallic iridium with an fcc structure [39]. Although the intensity of these reflections is very low, they are noticeable, particularly for the Ir-SiO-0F and Ir-SiO-2.0F catalysts. The presence of these reflections at such a low active phase loading (1 wt.%), may indicate crystallites with a size above 5 nm, however, such low intensity prevents a reliable Scherrer analysis. The reflection at $2\Theta = 40.6^\circ$ is particularly prominent for the Ir-SiO-0F catalyst. This suggests that the modification of the silica support leads to better dispersion of the active phase for catalysts with a modified support. The XRD results confirm the findings obtained from hydrogen chemisorption.

All iridium-modified catalysts were tested in liquid phase furfural hydrogenation (150°C, 20 bar, 2 h). After each test, the reaction solutions were tested on ICP in order to study the possible leaching of the Ir from the catalyst. In all cases, no leaching was observed. The results are presented in Fig. 7. All catalysts showed high activity with the conversion of furfural (FF) between 60 and 100% (Fig. 7**a**). The iridium catalysts on modified supports showed higher conversion in comparison to the catalyst on unmodified silica. The highest conversion was obtained for the Ir-SiO-1F catalyst. The selectivity profiles are presented in Fig. 7**b**. The main product in all cases was furfuryl alcohol (FFA). However, due to the acidity of the supports, the presence of various byproducts was also observed for Ir-SiO-0F, Ir-SiO-0.5F, and Ir-SiO-2.0F catalysts (e.g. tetrahydrofurfuryl alcohol, 2-methylfuran, furan–methanol ethers or minor amounts of levulinic acid derivatives). Interestingly, the most active catalyst (Ir-SiO-1.0) was also the most selective to furfuryl alcohol. In the case of furfural hydrogenation, one of the most important factors is the type of adsorption on the catalyst surface. The hydrogenation of furfural over iridium-based catalysts is highly sensitive to reaction conditions, particularly surface coverage and the resulting changes in adsorption geometry [40]. Similar to observations on Pt(111), FF can adopt different adsorption modes on iridium surfaces depending on the coverage. At low coverage, a planar geometry might be favoured, while higher coverage could lead to tilting and a more densely packed adlayer. These changes in adsorption mode directly influence product selectivity (**Fig. S4**). When furfural adsorbs primarily through the carbonyl moiety via an η^1-(O)-aldehyde or a tilted η^2-(C,O)-aldehyde configuration, the hydrogenation of the aldehyde group to furfuryl alcohol is favoured, leaving the furan ring largely unaffected. However, when furfural adopts a more planar η^2-(C, O)-aldehyde adsorption mode, where both the furan ring and the formyl group interact significantly with the iridium surface, hydrogenation of both functionalities becomes more likely, potentially leading to tetrahydrofurfuryl alcohol or other ring-hydrogenated products [40]. The specific strength of the Ir-furfural interaction and its influence on the preferred adsorption mode would dictate the initial steps of the reaction. Following the initial hydrogenation of the aldehyde to FFA, the presence of the hydroxymethyl group can further influence the adsorption on iridium surfaces, potentially favouring a more planar configuration, especially at defect sites like edges and corners. Similar to Pd, this planar adsorption could promote subsequent furan ring hydrogenation. The temperature also plays a crucial role in determining the dominant adsorption mode on iridium. Analogous to the other noble metal systems, such as Pd or Pt, higher temperatures might favour a different adsorption geometry compared to lower temperatures, potentially shifting the selectivity between FFA and THFFA. For instance, at higher temperatures, a configuration hindering furan ring interaction might

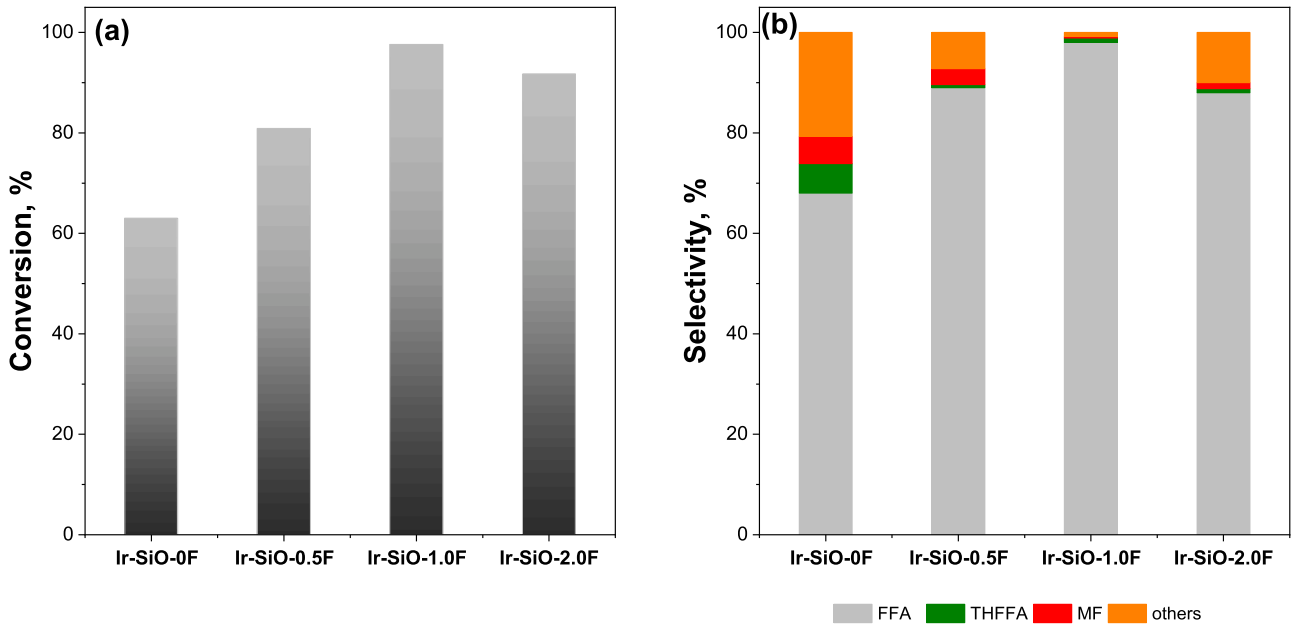

Fig. 7. Furfural hydrogenation on iridium catalysts: a) furfural conversion and b) product selectivity (150°C, 20 bar, 2 h, 50 mg of catalyst).

become more prevalent, favouring FFA formation. Conversely, lower temperatures could promote an adsorption mode conducive to both aldehyde and ring hydrogenation. Therefore, the selectivity of iridium-based catalysts in furfural hydrogenation can be tuned by carefully controlling reaction conditions such as temperature and surface coverage, which directly impact the dominant furfural adsorption mode. Understanding the precise nature of furfural adsorption on different iridium facets and under varying conditions is crucial for designing highly selective iridium catalysts for either FFA or THFFA production.

Taking high activity of Ir-based catalysts in furfural hydrogenation, we used XPS analysis to study the oxidation state of Ir in these materials. The results are summarized in Table 5 and Fig. 8. In all cases, four peaks are observed in the 4f region, which correspond to the Ir^0 and Ir^{4+} components. The results clearly indicate the highest Ir^0 to Ir^{4+} ratio for the catalyst supported on unmodified silica (Ir-SiO-0F). Similar ratios were observed for Ir-SiO-0.5F and Ir-SiO-2.0F samples, amounting to 0.79 and 0.78, respectively. Interestingly, the lowest ratio was observed in the case of the Ir-SiO-1.0F sample. This sample was also the most active and selective in the furfural hydrogenation. These results were confirmed by TPR-H_2 measurements of the samples after XPS analysis (**Fig. S5**). The reduction profiles exhibit maximum at 133°C, corresponding to the reduction of well-dispersed Ir^{4+}. In the case of the Ir-SiO-0F sample, the intensity of the peak at 133°C is small, indicating a low amount of Ir^{4+}, whereas for the Ir-SiO-1.0F sample, the intensity of the Ir^{4+} reduction peak is the highest. These findings are consistent with the results obtained from H_2 or CO chemisorption (Table 4) as well as from XPS analysis (Table 5).

A good correlation could be found between the Ir^0 to Ir^{4+} ratio and the selectivity to furfuryl alcohol, as shown in Fig. 9**a**. In addition, similar correlation can be found between Ir dispersion and the FFA selectivity (Fig. 9**b**). This may suggest that a dual-site mechanism could be responsible for the unique selectivity of the Ir-SiO-1.0F catalyst. It could be proposed that furfural is preferentially adsorbed on IrO_2 and then reduced by hydrogen dissociated on Ir^0 surface [41,42].

The XPS analysis, which provides quantified surface compositions and reduction profiles, indeed reveals crucial insights into the evolution of Ir oxidation states on the catalyst surface. It could be concluded that different iridium species directly contribute to the observed catalytic behavior, particularly in terms of selectivity. The findings suggest that the Ir^{4+} species, likely present as surface IrO_2, act as electron-deficient Lewis acid sites. These sites play a vital role in the preferential activation of the furfural molecule via C=O binding. This electronic interaction at the Ir^{4+} sites facilitates the hydrogenation of the carbonyl group, driving the selectivity towards furfuryl alcohol. We have also established that the balance (or ratio) of metallic Ir^0 to oxidized Ir^{4+} species on the catalyst surface is a key determinant of the reaction pathway.

This ratio dictates whether the hydrogenation reaction predominantly favors the reduction of the C=O bond (leading to furfuryl alcohol) or proceeds further to the hydrogenation of the C=C bond within the furan ring. The specific electronic environment provided by each oxidation state, and their relative abundance, therefore directly impact the observed selectivity. In addition, a strong linear correlation between the quantity of low temperature acid sites (Lewis acids) in the catalysts and the shift to lower BE in Ir^0 (Fig. 10) was observed. This clearly indicates that the modification of the silica with ammonium fluoride impacts the electronic properties of the iridium. The shift of the BE to lower binding energy is probably due to the electron migration to iridium. It could also be due to electrostatic interactions and it is not due to the Ir particle size changes, as any correlation in this case was observed.

The activity and the selectivity are strongly influenced by the balanced ratio of acidity and Ir dispersion. First of all, the NH_4F treatment enables a reduction in the average Ir particle size, leading to better dispersion of the active metal sites. The introduction of fluoride allows for precise control over the ratio of metallic Ir^0 to oxidized Ir^{4+} species on the surface. Studies show that low Ir-loading samples (e.g., 1%Ir/SiO_2) predominantly contain surface Ir^{4+} species, while higher loadings (e.g., 3%Ir/SiO_2, 5%Ir/SiO_2) exhibit a mixture of Ir^0 and Ir^{4+} [13]. The best catalytic results were observed for the 3%Ir which presented also the higher Ir^0 to Ir^{4+} ratio. Modification of silica with ammonium fluoride modulates also its surface acid sites. A proper Ir^{4+}/Ir^0 ratio is crucial for the chemisorption and activation of the aldehyde moiety,

Table 5
XPS analysis and Ir^0/Ir^{4+} XPS atomic ratio.

Catalyst	Ir total [%]	Ir^0 [%]	Ir^{4+} [%]	Ir^0/Ir^{4+}
Ir-SiO–0F	0.05	74.15	25.85	2.86
Ir-SiO–0.5F	0.08	42.95	57.06	0.79
Ir-SiO–1.0F	0.06	27.44	72.56	0.38
Ir-SiO–2.0F	0.05	44.05	55.95	0.78

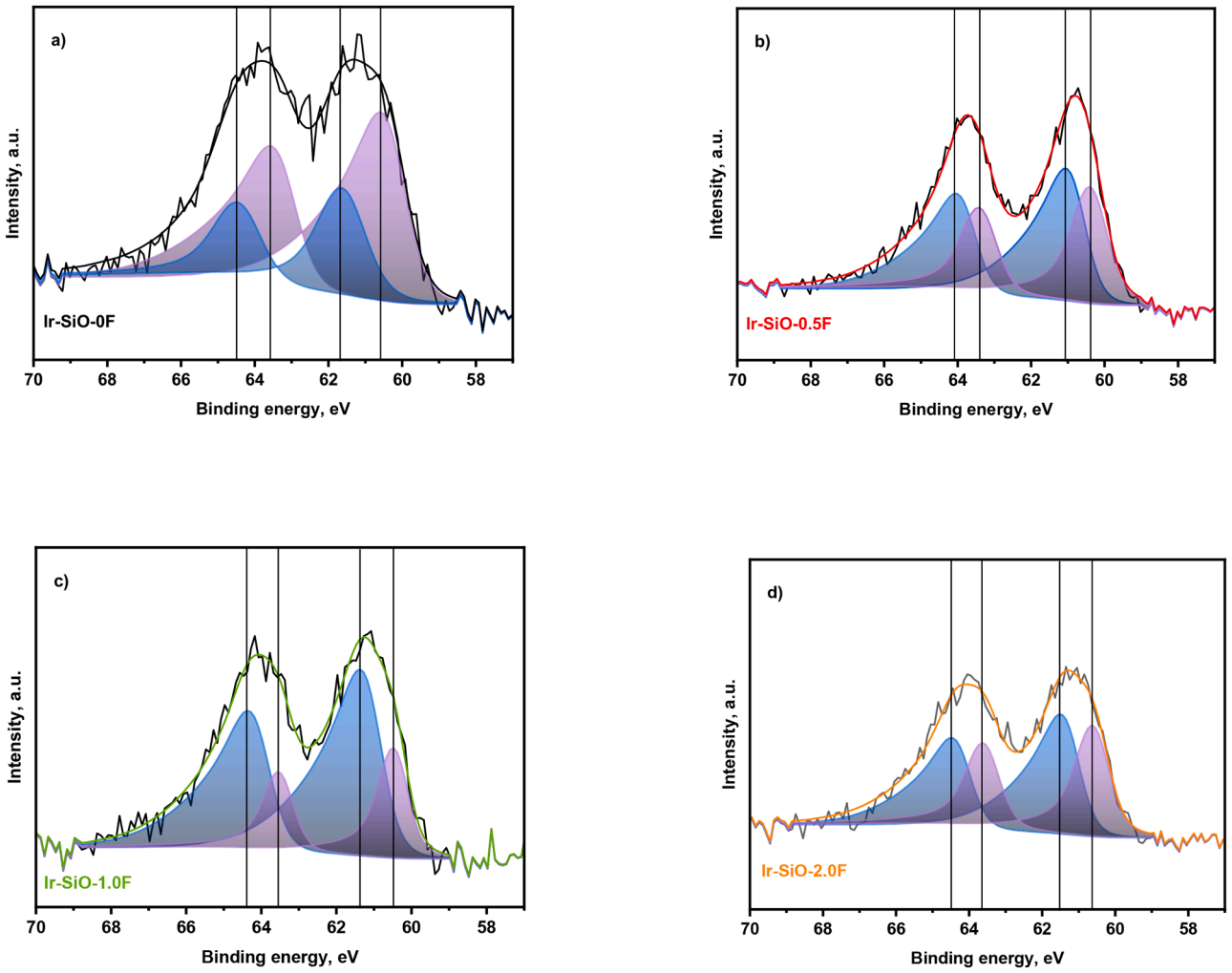

Fig. 8. XPS narrow spectra for Ir 4f region for indicated Ir based catalysts a) Ir-SiO-0F, b) Ir-SiO-0.5F, c) Ir-SiO-1.0F, d) Ir-SiO-2.0F.

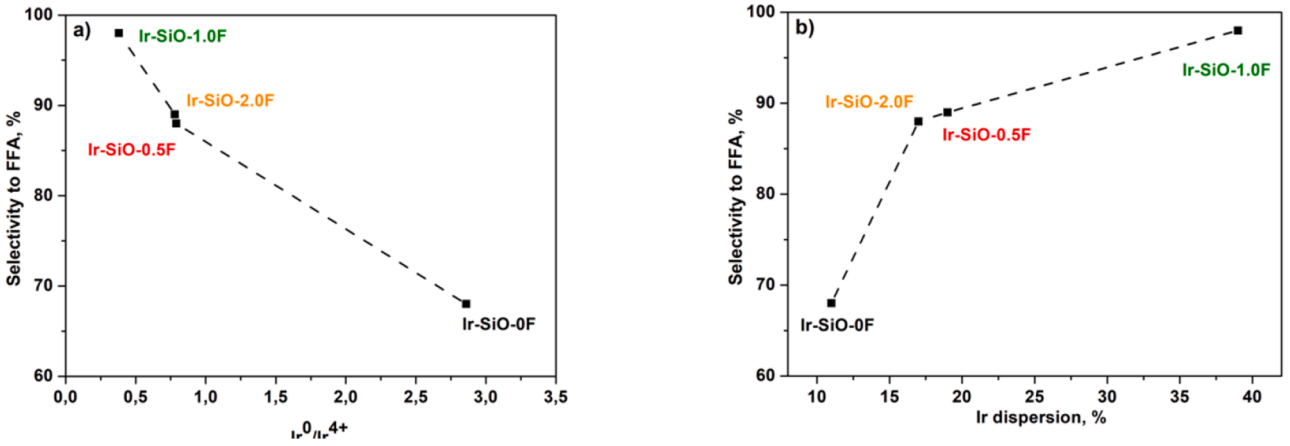

Fig. 9. Selectivity to FFA versus Ir^0/Ir^{4+} atomic ratio obtained from XPS data (a) and versus Ir dispersion calculated from the irreversibly adsorbed hydrogen (b).

leading to high hydrogenation activity. Lewis acid sites are proposed to interact with the carbonyl oxygen, while Ir^0 or partially reduced Ir^+ species serves as the adsorption center for the C-C bond and carbonyl carbon [15]. Increased surface Lewis acidity and enhanced Ir dispersion, particularly with higher ammonium fluoride amounts, provide more sites for carbonyl oxygen adsorption and facilitate chemisorption on Ir^0 sites, boosting reactivity. The selectivity is also found to be influenced by the Ir^0/Ir^{4+} ratio. While surface Lewis acidity is vital for carbonyl oxygen chemisorption and desirable alcohol formation, an excess of Lewis acid sites can lead to strong C-C bond interaction with Ir^0 sites, potentially hindering selectivity. High acidity has also been linked to increased coking and deactivation in selective hydrogenation [43].

To gain a deeper understanding of the structure-activity and selectivity relationship of the tested iridium-based catalysts in furfural

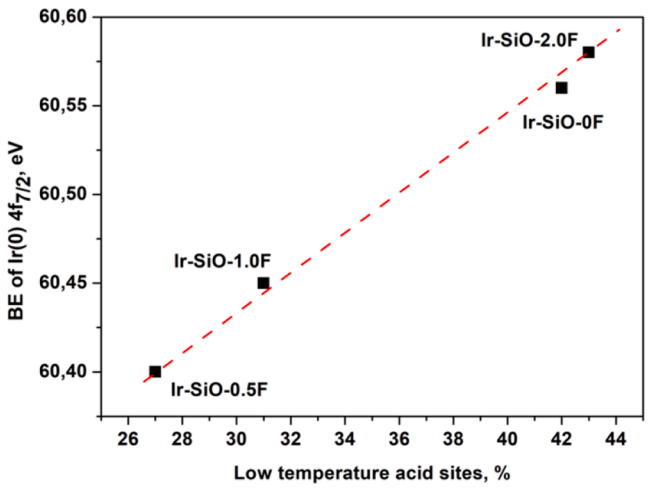

Fig. 10. Correlation between the low temperature acid sites and the shift of BE in Ir^0 $4f_{7/2}$ region.

hydrogenation, DFT simulations were employed as a hypothesis-driven tool to validate and mechanistically explain our experimental observations. Our experimental findings revealed a strong correlation between the Ir^0/Ir^{4+} ratio on the catalyst surface and the selectivity towards either THFA or FFA. Specifically, an increased presence of metallic Ir favored THFA production, while higher Ir^{4+} content promoted FFA formation. The DFT analysis provided atomic-level insights that directly support these experimental trends. By modeling furfural adsorption on both metallic Ir(111) and oxidized IrO_2(110) surfaces, our simulations demonstrated distinct preferred adsorption modes and bond activation patterns. The results of these simulations are presented in Figs 11 and 12, which provide valuable insights into the preferred adsorption modes of furfural on the iridium surfaces and their correlation with the experimentally observed product distribution. From XPS, we could observe that varying the Ir^0/Ir^{4+} ratio, different selectivity was obtained. In order to explain this result, we modelled the two most commonly exposed facets of metallic Ir nanoparticles and IrO_2, namely (111) and (110) planes, in order to obtain insights into their structural and electronic differences [44–48]. The structural and electronic differences of these surfaces are crucial to explain the different results obtained by varying the Ir^0/Ir^{4+} ratio in terms of catalytic behavior. The DFT simulations were performed by using the Perdew-Burke-Ernzerhof (PBE) functional [19], including dispersion forces as implemented by Grimme with Becke-Johnson damping function [49], which is a reasonable choice for studying adsorption on metal and metal oxide surfaces [50,51]. Then, furfural was adsorbed on the non-equivalent

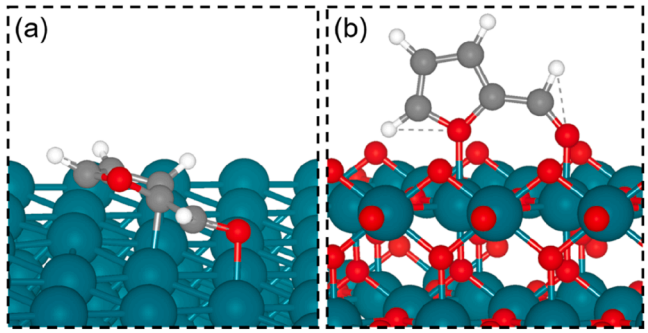

Fig. 12. Structures of the most stable adsorption modes of furfural on (a) Ir (111) and (b) IrO_2(110) (red-oxygen atoms, grey-carbon atoms, green-iridium atoms).

sites of the slabs and with a different conformation. The binding energies for each structure were calculated as a difference with the energy of the free *trans*-furfural and surface (according to Eq. (6)). The binding energies and structure parameters of all the different species adsorbed on the two surfaces considered can be found in **Table S2** and **S3**, in the Supporting Information. Both *cis* and *trans* furfural were modelled in the gas phase, and in agreement with other works, the *trans* conformer was found to be the most stable [52,53]. However, the energy difference between the two structures is low (less than 0.05 eV), and for this reason, in the reaction environment, both *cis* and *trans* forms are considered to be present. Furfural, either *trans*- or *cis*-, can be adsorbed parallel to the surface, indicated as flat, or in a perpendicular way to the slab plane, named top. An intermediate configuration between these two is possible and considered in this study, namely tilted, see Fig. 11 [52].

Fig. 12 shows the most stable conformation obtained for each surface. Comparing the optimized model, it is to be noted that two very different adsorption modes were obtained. Indeed, on Ir(111), furfural is strongly adsorbed parallel to the metal surface with a binding energy of -2.029 eV. Herein, the C=O bond is elongated by 0.12 Å, from 1.23 to 1.35 Å, closer to the length of a C-O bond. This indicated an activation of the bond, which can be easily hydrogenated to C-OH. It is worth mentioning that the C=C bonds of the furanic rings were activated, the bond length varied by 0.12 Å, passing from approximately 1.38 Å to 1.50 Å. This seems to corroborate the idea that catalysts containing a high percentage of Ir° can more easily lead to products presenting both the carbonyl and the furanic ring reduced, i.e., THFA (Fig. 12**a**). This is supported by the experimental findings, where an increased amount of Ir^0 enhanced the production of tetrahydrofurfuryl alcohol. Indeed, Ir NPs supported on SiO-0F presented the high amount of Ir^0 (74.15%) leading to the formation of either FFA and THFFA, see Fig. 7 and Table 5. The situation is different when FF interacts with IrO_2(110). Here, the

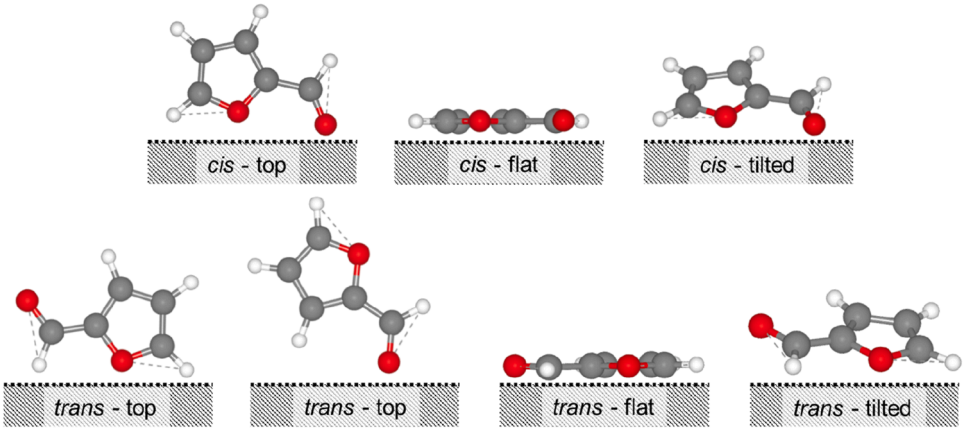

Fig. 11. Schematic representation of the different adsorption modes of *cis*- and *trans*-furfural on the considered surfaces.

molecule adsorbs perpendicularly on the unsaturated $Ir^{\delta+}$ of the surface with the oxygen atoms from the carbonyl group and the furanic ring (ΔE of -2.476 eV, see Fig. 12**b**). The difference in binding energy between the Ir (111) and IrO_2 (110) surface of about 0.5 eV indicates a preferential adsorption of FF on the metal oxide. From the selectivity point of view, the modelling also corroborates the correlation between the catalytic data and the surface characterization obtained from XPS. Indeed, such perpendicular interaction favors the hydrogenation of the carbonyl group, without modification of the furanic ring, thus explaining the enhanced formation of FFA in the presence of IrO_2, as in the case of Ir-SiO–1.0F catalyst having a Ir^0/Ir^{4+} ratio of 0.38 and giving the highest selectivity for FFA, near 100 % (Fig. 7 and Table 5).

Thus, DFT served not merely as a descriptive tool, but as a crucial theoretical framework that allowed us to formulate and then validate hypotheses about the specific roles of different iridium oxidation states in governing reaction selectivity, transforming empirical correlations into a well-understood structure-activity relationship.

4. Conclusions

The modification of amorphous silica with ammonium fluoride effectively altered its textural and acidic properties. This treatment led to partial silicon leaching, an increase in pore size and volume, and enhanced surface acidity, while still maintaining a relatively high surface area. The acidity characterization (TPD-NH_3 and FTIR-Py) revealed that the modification increases the number of acid sites, particularly weak Lewis acid sites, with the highest saturation achieved at a NH_4F concentration of 1.0 M. The sample SiO-1.0F exhibited the most favourable textural and acidic properties, as reflected by a beneficial ratio of specific surface area to the number of acid sites, which resulted in the highest iridium dispersion and the smallest nanoparticle size in the corresponding catalyst. Iridium catalysts on silica supports modified with ammonium fluoride showed high activity in the hydrogenation of furfural, with the Ir-SiO-1.0F catalyst achieving the highest activity and selectivity toward furfuryl alcohol. XPS and TPR-H_2 studies indicated a significant role of the Ir^0/Ir^{4+} ratio in shaping catalyst selectivity, suggesting a dual-site mechanism in which furfural is adsorbed on IrO_2 while reduction occurs via H_2 activated on the Ir^0 surface. DFT calculations supported the experimental observations, revealing distinct adsorption modes of furfural depending on the oxidation state and facet type of iridium, which in turn influence the reaction pathway and product selectivity.

CRediT authorship contribution statement

Robert Wojcieszak: Writing – original draft, Validation, Supervision, Conceptualization. **Monika Kot:** Investigation, Formal analysis, Data curation. **Arthur Reymond:** Writing – review & editing, Data curation. **Camila Palombo Ferraz:** Formal analysis, Data curation, Conceptualization. **Nikolaos Dimitratos:** Writing – review & editing, Methodology, Investigation. **Alberto Villa:** Writing – review & editing, Investigation, Data curation. **Ilaria Barlocco:** Writing – review & editing, Data curation. **Silvio Bellomi:** Writing – review & editing, Data curation. **Mariusz Pietrowski:** Writing – review & editing, Methodology, Formal analysis. **Ewa Janiszewska:** Writing – review & editing, Writing – original draft, Methodology. **Michał Zieliński:** Writing – review & editing, Validation, Conceptualization. **Almudena Marti:** Writing – review & editing, Validation, Supervision.

Declaration of competing interest

The authors declare that they have no known competing financial interests or personal relationships that could have appeared to influence the work reported in this paper.

Supplementary materials

Supplementary material associated with this article can be found in the online version at doi:10.1016/j.apmt.2025.102929.

Data availability

Data will be made available on request.

References

[1] D. Pandey, G. Deo, Effect of support on the catalytic activity of supported Ni–Fe catalysts for the CO_2 methanation reaction, J. Indust. Eng. Chem. 33 (2016) 99–107.

[2] N. Dimitratos, G. Vilé, S. Albonetti, F. Cavani, J. Fiorio, N. López, L.M. Rossi, R. Wojcieszak, Chemical aspects in hydrogenation on gold nanocatalysts, Nat. Rev. Chem. 8 (2024) 195–210.

[3] J. Ye, N. Dimitratos, L. Rossi, A. Baele, N. Thonneman, R. Wojcieszak, Hydrogenation of CO_2 for sustainable fuel and chemical production, Science 387 (2025) 6737.

[4] I. Pulido-Diaz, A. Serrando-Maldonado, C.L. Suarez, P.M. Ocampo, B.P. Martinez, A. Gutierrez Alejandre, K. Salas Martin, I.G. Rios, RhNPs supported on N-functionalized mesoporous silica: effect on catalyst stabilization and catalytic activity, Dalton. Trans. 50 (2021) 3289–3298.

[5] M. Kot, R. Wojcieszak, E. Janiszewska, M. Pietrowski, M. Zielinski, Effect of modification of amorphous silica with ammonium agents on the physicochemical properties and hydrogenation activity of Ir/SiO2 catalysts, Materials. 14 (2021) 968.

[6] M. Guisnet, P. Magnoux, Coking and deactivation of zeolites: influence of the pore structure, Appl. Catal. 54 (1989) 1–27.

[7] C. Ferraz, M. Pietrowski, M. Zielinski, S. Heyte, L. Rossi, F. Dumeignil, R. Wojcieszak, Influence of support basic sites in green oxidation of biobased substrates using Au-promoted catalysts, ACS Sustain. Chem. Eng. 6 (2018) 16332–16340.

[8] D. Shi, A. Sadier, JS. Girardon, A.S. Mamede, C. Ciotonea, M. Marinova, L. Stievano, M.T. Sougrati, C. La Fontaine, S. Paul, R. Wojcieszak, E. Marceau, Probing the core and surface composition of nanoalloy to rationalize its selectivity: the case of Ni-Fe/SiO_2 catalysts for liquid-phase hydrogenation, Chem. Catal. 2 (2022) 1686–1708.

[9] (Accessed on 29th of April, http://minafin.com/origin-materials-and-minafin-group-form-strategic-partnership-to-industrialize-carbon-negative-chemicals-and-materials/, 2025 (Accessed on 29th of April.

[10] M. Zielinski, M. Kot, M. Pietrowski, R. Wojcieszak, J.K. Kus, E. Janiszewska, Studies of new iridium catalysts supported on modified silicalite-1—their structure and hydrogenating properties, Materials. 14 (2021) 4465.

[11] J. Lu, P. Serna, C. Aydin, N. Browning, B. Gates, Supported molecular iridium catalysts: resolving effects of metal nuclearity and supports as ligands, J. Am. Chem. Soc. 133 (40) (2011) 16186–16195.

[12] Z. Amirsardari, A. Dourani, F. Hasanpour, M. Ali Amirifar, N. Massoom, Effect of silica content on support-iridium active phase interactions on the nanocatalyst activity, J. Nanostruct. 10 (2020) 348–361.

[13] X. Hong, B. Li, Y. Wang, J. Lu, G. Hu, M. Lu, Stable Ir/SiO2 catalyst for selective hydrogenation of crotonaldehyde, Appl. Surf. Sci. 270 (2013) 388–394.

[14] P. Chen, J-Q. Lu, G. Xie, G. Hu, L. Zhu, L. Luo, W. Huang, M. Luo, Effect of reduction temperature on selective hydrogenation of crotonaldehyde over Ir/TiO2 catalysts, Appl. Catal. A. Gen. 433-434 (2012) 236–242.

[15] L. Zhu, G. Hu, J. Lu, G. Xie, P. Chen, M. Luo, Effects of Ir content on selective hydrogenation of crotonaldehyde over Ir/ZrO2 catalysts, Catal. Comm. 21 (2012) 5–8.

[16] H. Ertl, F. Knözinger, J. Schüth, Weitkamp, handbook of heterogeneous catalysis, Wiley VCH 8 (2008).

[17] G. Kresse, Ab initio molecular dynamics for liquid metals, J. Non Cristal. Solids 192 (1995) 222–229.

[18] G. Kresse, D. Joubert, From ultrasoft pseudopotentials to the projector augmented-wave method, Phys. Rev. 59 (1999) 1758.

[19] J. Perdew, K. Burke, M. Ernzerhof, Generalized gradient approximation made simple, Phys. Rev. Lett 77 (1996) 3865–3868.

[20] J.-X. Liu, Y. Su, I.A.W. Filot, E.J.M. Hensen, A linear scaling relation for CO oxidation on CeO2-supported Pd, J. Am. Chem. Soc. 140 (2018) 4580–4587.

[21] J. Pack, H. Monkhorst, Special points for Brillouin-zone integrations"—a reply, Phys. Rev. B 16 (1977) 1748.

[22] A.H. Larsen, J.J. Mortensen, J. Blomqvist, I.E. Castelli, R. Christensen, M. Dułak, J. Friis, M.N. Groves, B. Hammer, C. Hargus, The atomic simulation environment—a python library for working with atoms, J. Phys. Condens. Matter. 29 (2017) 273002.

[23] S. Bellomi, D.C. Cano-Blanco, I. Barlocco, J.J. Delgado, X. Chen, L. Prati, D. Ferri, N. Dimitratos, A. Roldan, A. Villa, Probing the metal/oxide interface of IrCoCeO x in N2H4· H2O decomposition: an experimental and computational study, ACS. Appl. Mater. Interfaces. 16 (40) (2024) 54897–54906.

[24] S. Bellomi, I. Barlocco, X. Chen, J.J. Delgado, R. Arrigo, N. Dimitratos, A. Roldan, A. Villa, Enhanced stability of sub-nanometric iridium decorated graphitic carbon nitride for H2 production upon hydrous hydrazine decomposition, Phys. Chem. Chem. Phys. 25 (2023) 1081–1095.

[25] R. Sure, J. Antony, S. Grimme, Blind prediction of binding affinities for charged supramolecular host–guest systems: achievements and shortcomings of DFT-D3, J. Phys. Chem. B 118 (2014) 3431–3440.
[26] S. Ehrlich, J. Moellmann, W. Reckien, T. Bredow, S. Grimme, System-dependent dispersion coefficients for the DFT-D3 treatment of adsorption processes on ionic surfaces, Chemphyschem. 12 (2011) 3414–3420.
[27] H. Fang, A. Roldan, C. Tian, Y. Zheng, X. Duan, K. Chen, L. Ye, S. Leoni, Y. Yuan, Structural tuning and catalysis of tungsten carbides for the regioselective cleavage of csingle bondO bonds, J. Catal. 369 (2019) 282–295.
[28] X. Lu, S. Francis, D. Motta, N. Dimitratos, A. Roldan, Mechnaistic study of hydrazine decomposition on Ir(111), Phys. Chem. Chem. Phys. 22 (2020) 3883–3896.
[29] E. Janiszewska, J. Kowalska-Kuś, K. Góra-Marek, A. Szymocha, K. Nowińska, S. Kowalak, Modification of silicalite-1 with ammonium compounds aimed at preparation of acidic catalyst for acetalization of glycerol with acetone, Appl. Catal. A. General 581 (2019) 1–10.
[30] M. Thommes, K. Kaneko, A.V. Neimark, J.P. Olivier, F. Rodriguez-Reinoso, J. Rouquerol, K.S.W. Sing physisorption of gases, with special reference to the evaluation of surface area and pore size distribution (IUPAC Technical Report), Pure Appl. Chem. 87 (9-10) (2015) 1051–1069, https://doi.org/10.1515/pac-2014-1117.
[31] F. Lónyi, J. Valyon, On the interpretation of the NH_3-TPD patterns of H-ZSM-5 and H-mordenite, Microporous Mesoporous Mater 47 (2001) 293–301, https://doi.org/10.1016/S1387-1811(01)00389-4.
[32] E. Janiszewska, M. Kot, M. Zieliński, Modification of silica with NH4+ agents to prepare an acidic support for iridium hydrogenation catalyst, Microporous Mesoporous Mater 255 (2018) 94–102.
[33] P. Lanzafame, K. Barbera, S. Perathoner, G. Centi, A. Aloise, M. Migliori, A. Macario, J. Nagy, G. Giordano, The role of acid sites induced by defects in the etherification of HMF on Silicalite-1 catalysts, J. Catal. 330 (2015) 558–568.
[34] M.I. Zaki, M.A. Hasan, F.A. Al-Sagheer, L. Pasupulety, In situ FTIR spectra of pyridine adsorbed on SiO_2–Al_2O_3, TiO_2, ZrO_2 and CeO_2: general considerations for the identification of acid sites on surfaces of finely divided metal oxides, Colloids. Surf. a Physicochem. Eng. Asp. 190 (2001) 261–274, https://doi.org/10.1016/S0927-7757(01)00690-2.
[35] H. Hattori, P. Arudra, A. Abdalla, A.M. Aitani, A.S.S. l-Khattaf, Infrared study of silanol groups on dealuminated high silica MFI zeolite to correlate different types of silanol groups with activity for conversion of 1-butene to propene, Catal. Lett. 150 (2020) 771–780, https://doi.org/10.1007/s10562-019-02972-8.
[36] Y. Li, W. Zhang, L. Zhang, Q. Yang, Z. Wie, Z. Feng, C. Li, Direct synthesis of Al−SBA-15 mesoporous materials via hydrolysis-controlled approach, J. Phys. Chem. B 108 (2004) 9739–9744, https://doi.org/10.1021/jp049824j.
[37] R.J. Silvennoinen, O.J.T. Jylhä, M. Lindblad, H. Österholm, A.O.I. Krause, Supported iridium catalysts prepared by atomic layer deposition: effect of reduction and calcination on activity in toluene hydrogenation, Catal. Lett. 114 (3–4) (2007) 135–144, https://doi.org/10.1007/s10562-007-9051-7.
[38] O. Hernández-Cristóbal, G. Díaz, A. Gómez-Cortés, Effect of the reduction temperature on the activity and selectivity of titania-supported iridium nanoparticles for methylcyclopentane reaction, Ind. Eng. Chem. Res. 53 (2014) 10097–10104, https://doi.org/10.1021/ie501283c.
[39] International center for diffraction data (https://www.icdd.com): JCPDS PDF#06-0598.
[40] S. Chen, R. Wojcieszak, F. Dumeignil, E. Marceau, S. Royer, How catalysts and experimental conditions determine the selective hydroconversion of furfural and 5-hydroxymethylfurfural, Chem. Rev. 118 (2018) 11023–11117, https://doi.org/10.1021/acs.chemrev.8b00134.
[41] S. Kim, H. Jung, C. Lee, M. Kim, Y. Lee, Comparative study on hydrogen evolution reaction activity of electrospun nanofibers with diverse metallic Ir and IrO2 composition ratios, ACS Sustainable Chem. Eng. 7 (9) (2019) 8613–8620.
[42] D. Aireddy, K. Ding, Heterolytic dissociation of H_2 in heterogeneous catalysis, ACS. Catal. 12 (8) (2022) 4707–4723.
[43] X. Wang, H. Zheng, X. Liu, G. Xie, J. Lu, L. Jin, M. Luo, Effects of NaCl on Pt/ZrO2 catalysts for selective hydrogenation of crotonaldehyde, Appl. Catal. A Gen. 388 (2010) 134–140.
[44] J. Kua, F. Faglioni, W. Goddard, Thermochemistry for hydrocarbon intermediates chemisorbed on metal surfaces: CHn-m(CH3)m with $n = 1, 2, 3$ and $m \leq n$ on Pt, Ir, Os, Pd, Rh, and Ru, J. Am. Chem. Soc. 122 (10) (2000) 2309–2321.
[45] Y. Ping, R. Nielsen, W. Goddard, The reaction mechanism with free energy barriers at constant potentials for the oxygen evolution reaction at the IrO2 (110) surface, J. Am. Chem. Soc. 139 (1) (2017) 149–155.
[46] K. Exner, H. Over, Beyond the rate-determining step in the oxygen evolution reaction over a single-crystalline IrO2(110) model electrode: kinetic scaling relations, ACS. Catal. 9 (8) (2019) 6755–6765.
[47] H. Zhang, A. Soon, B. Delley, C. Stampfl, Stability, structure, and electronic properties of chemisorbed oxygen and thin surface oxides on Ir(111), Phys. Rev. B 78 (2008) 045436.
[48] W. Krekelberg, J. Greeley, M. Mavrikakis, Atomic and molecular adsorption on Ir (111), J. Phys. Chem. B 108 (3) (2004) 987–994.
[49] S. Grimme, S. Ehrlich, L. Goerigk, Effect of the damping function in dispersion corrected density functional theory, J. Comp. Chem. 32 (2011) 1456–1465.
[50] P. Janthon, S. Kozlov, F. Vines, J. Limtakul, F. Illas, Establishing the accuracy of broadly used density functionals in describing bulk properties of transition metals, J. Chem. Theory. Comput. 9 (3) (2013) 1631–1640.
[51] V. Ruta, L. Cipriano, G. De Libertà, R. Wojcieszak, G. Vilé, Bifunctional Pd-Pt supported nanoparticles for the mild hydrodeoxygenation and oxidation of biomass-derived compounds, ChemSusChem. (2025) e20242641.
[52] S. Pang, W. Medlin, Adsorption and reaction of furfural and furfuryl alcohol on Pd (111): unique reaction pathways for multifunctional reagents, ACS. Catal. 1 (10) (2011) 1272–1283.
[53] B. Liu, L. Cheng, L. Curtiss, J. Greeley, Effects of van der Waals density functional corrections on trends in furfural adsorption and hydrogenation on close-packed transition metal surfaces, Surf. Sci. 622 (2014) 51–59.